

Tetraspanin CD9 stabilizes gp130 by preventing its ubiquitin-dependent lysosomal degradation to promote STAT3 activation in glioma stem cells

Yu Shi^{1,2,3}, Wenchao Zhou¹, Lin Cheng⁴, Cong Chen^{1,2,3}, Zhi Huang¹, Xiaoguang Fang¹, Qiulian Wu¹, Zhicheng He^{2,3}, Senlin Xu^{2,3}, Justin D Lathia⁵, Yifang Ping^{2,3}, Jeremy N Rich¹, Xiu-Wu Bian^{*2,3} and Shideng Bao^{*1}

Glioblastoma (GBM) is the most malignant and lethal brain tumor harboring glioma stem cells (GSCs) that promote tumor propagation and therapeutic resistance. GSCs preferentially express several critical cell surface molecules that regulate the pro-survival signaling for maintaining the stem cell-like phenotype. Tetraspanin CD9 has recently been reported as a GSC biomarker that is relevant to the GSC maintenance. However, the underlying molecular mechanisms of CD9 in maintaining GSC property remain elusive. Herein, we report that CD9 stabilizes the IL-6 receptor glycoprotein 130 (gp130) by preventing its ubiquitin-dependent lysosomal degradation to facilitate the STAT3 activation in GSCs. CD9 is preferentially expressed in GSCs of human GBM tumors. Mass spectrometry analysis identified gp130 as an interacting protein of CD9 in GSCs, which was confirmed by immunoprecipitation and immunofluorescent analyses. Disrupting CD9 or gp130 by shRNA significantly inhibited the self-renewal and promoted the differentiation of GSCs. Moreover, CD9 disruption markedly reduced gp130 protein levels and STAT3 activating phosphorylation in GSCs. CD9 stabilized gp130 by preventing its ubiquitin-dependent lysosomal degradation to promote the BMX-STAT3 signaling in GSCs. Importantly, targeting CD9 potently inhibited GSC tumor growth *in vivo*, while ectopic expression of the constitutively activated STAT3 (STAT3-C) restored the tumor growth impaired by CD9 disruption. Collectively, we uncovered a critical regulatory mechanism mediated by tetraspanin CD9 to maintain the stem cell-like property and tumorigenic potential of GSCs.

Cell Death and Differentiation (2017) 24, 167–180; doi:10.1038/cdd.2016.110; published online 14 October 2016

Glioblastoma (GBM) is the most common and aggressive primary brain tumor with dismal prognosis.^{1,2} Despite recent advance in the treatment of other cancers, current therapies for GBM remain palliative.² GBM is featured by the remarkable cellular heterogeneity and differential hierarchies of cancer cells. Growing evidence supported that a subset of cancer cells, referred to as glioma stem cells (GSCs) or tumor initiating cells, are responsible for tumor propagation and recurrence in GBMs.^{3–5} Although the cellular origin of GSCs remains controversial,⁶ these cells have been demonstrated to share several typical features of embryonic or somatic stem cells (i.e., self-renewal capacity and multi-lineage differentiation potential). GSCs are privileged to drive tumor initiation and malignant progression.^{6,7} The potent capacity of GSCs in promoting tumor progression may be a result of their extensive potential to maintain cell proliferation and to support malignant

behaviors such as cancer invasion, tumor angiogenesis, vascular pericyte generation and immune evasion.^{5,8}

GSCs have been found to be enriched in GBMs after radiation and chemotherapy, and contribute to therapeutic resistance and tumor re-initiation.^{3,9} The pivotal role of GSCs in promoting malignant progression and tumor recurrence in GBMs indicate that targeting GSCs may significantly improve GBM treatment and overcome the therapeutic resistance. Thus, identifying key molecular regulators that control GSC self-renewal and tumorigenic potential may provide useful targets for the development of new therapeutic strategies to effectively improve GBM treatment. Cell surface molecules that are preferentially expressed in GSCs and regulate critical signaling for GSC maintenance are particularly amenable to specific targeting for the development of effective therapeutics against GSCs.

¹Department of Stem Cell Biology and Regenerative Medicine, Lerner Research Institute, Cleveland Clinic, Cleveland, OH 44195, USA; ²Institute of Pathology and Southwest Cancer Center, Southwest Hospital, The Third Military Medical University, Chongqing 400038, China; ³The Key Laboratory of Tumor Immunopathology, Ministry of Education of China, Chongqing 400038, China; ⁴State Key Laboratory of Medical Genomics, Shanghai Institute of Hematology, Rui Jin Hospital, Shanghai Jiao Tong University, Shanghai 200025, China and ⁵Department of Cellular and Molecular Medicine, Lerner Research Institute, Cleveland Clinic, Cleveland, OH 44195, USA

*Corresponding author: S Bao, Department of Stem Cell Biology and Regenerative Medicine, Cleveland Clinic, 9500 Euclid Avenue, Mail Stop NE30, Cleveland, OH 44195, USA. Tel: +1 216 636 1009; Fax: +1 216 636 5454; E-mail: baos@ccf.org

or X-W Bian, Institute of Pathology and Southwest Cancer Center, Southwest Hospital, The Third Military Medical University, and the Key Laboratory of Tumor Immunopathology, Ministry of Education of China, Chongqing 400038, China. Tel: +862368754431; Fax: +862368754431; E-mail: bianxiuwu@263.net

Abbreviations: BMX, bone marrow X-linked non-receptor tyrosine kinase; CD133 (Prominin 1), cell surface antigen AC133; CD15 (SSEA-1), stage-specific embryonic antigen 1; CD44, cell surface glycoprotein CD44; CD9, CD9 antigen (P24); CHL, chloroquine; EGF, epidermal growth factor; ES, embryonic stem cells; GBM, glioblastoma; GFAP, glial fibrillary acidic protein; gp130, glycoprotein 130; GSCs, glioma stem cells; IL-6, interleukin-6; LIF, leukemia inhibitory factor; MAP2, microtubule associated protein 2; N2C, non-stem tumor cell; OLIG2, oligodendrocyte lineage transcription factor 2; shRNA, short hairpin RNA; SOX2, SRY-related HMG-Box gene 2; STAT3, signal transducer and activator of transcription 3; STAT3-C, constitutively activated STAT3; TUNEL, terminal deoxynucleotidyl transferase dUTP nick end labeling

Received 18.2.16; revised 29.8.16; accepted 12.9.16; Edited by P Salomoni; published online 14.10.16

Tetraspanins are a family of cell surface glycoproteins, which couple multiple trans membrane receptors to function as key signal organizers or regulators.^{10,11} Tetraspanins are featured by four transmembrane domains that form multimeric complexes with other cell surface proteins to modulate diverse cellular processes, including cell fusion, adhesion and motility.^{10,12} To investigate the role of tetraspanins in the GSC maintenance, we screened for the tetraspanins preferentially expressed in GSCs relative to non-stem tumor cells (NSTCs) and identified tetraspanin CD9 as a GSC-enriched protein. As a key member of the tetraspanin family, CD9 is closely associated with malignant progression in a context-dependent manner. CD9 has a pro-tumorigenic role to promote cancer invasion and tumor growth in cervical cancer, gastric cancer and GBM.^{13–15} In addition, CD9 expression has potential prognostic value to predict patient survival.¹⁶ Moreover, CD9 is associated with the stem cell phenotype in embryonic stem cells (ES) and hematopoietic stem cells.^{17–19} Recently, CD9 has been shown to facilitate cell proliferation and tumorsphere formation of GSCs.¹⁵ However, the molecular mechanisms underlying the CD9 function in GSC maintenance have not been elucidated.

In this study, we used mass spectrometry (MS) analysis to screen for the potential CD9-interacting proteins and identified the interleukin-6 (IL-6) receptor subunit gp130 (glycoprotein 130) as a critical binding partner of CD9 in GSCs. Gp130 has a critical role in mediating IL-6 signaling. Upon the binding of IL-6 to IL-6R α , gp130 dimerizes and triggers a signal transduction to induce STAT3 (signal transducer and activator of transcription 3) phosphorylation (p-Tyr705), resulting in nuclear translocation of STAT3 and the active transcription of the STAT3 downstream genes responsible for cancer cell proliferation, invasion and tumor angiogenesis.^{20,21} The crucial role of the STAT3 activation in maintaining GSC property has been demonstrated by our laboratory and others.^{21–24} We previously showed that the non-receptor tyrosine kinase bone marrow X-linked non-receptor tyrosine kinase (BMX) mediates STAT3 hyper-activation in GSCs and demonstrated that the BMX-mediated STAT3 activation is required for maintaining GSC self-renewal and tumorigenic potential.²² However, how BMX kinase is activated by upstream regulators in this pivotal pathway remains elusive. Herein we demonstrate that CD9 stabilizes gp130 by blocking its ubiquitin-dependent lysosomal degradation to promote the IL6-gp130-BMX-STAT3 signaling for maintaining GSC self-renewal and tumorigenic capacity. Our study highlights CD9 as a crucial signal organizer for the gp130-mediated signal transduction in GSCs, indicating that CD9 is a potential target for the development of new therapeutics against GSCs to improve GBM treatment.

Results

Tetraspanin CD9 is preferentially expressed in GSCs. As tetraspanins have been implicated in tumor malignant progression,^{10,11} we sought to identify specific tetraspanins that are preferentially expressed in GSCs and investigate their functional significance in GSC maintenance and tumor growth. We used the published microarray profiles to analyze

tetraspanin expressions between GSCs ($n=12$) and conventional glioma cell lines (CGCs) ($n=32$) isolated from human GBMs (Gene Expression Omnibus; GEO: GDS3885).²⁵ We found that 4 out of 31 members of the tetraspanin family, *CD9*, *TSPAN7*, *TSPAN11* and *TSPAN33*, were significantly upregulated in GSCs relative to CGCs ($P<0.05$) (Figure 1a). The expressions of these candidates were further examined in 6 pairs of matched GSCs (CD15⁺/CD133⁺) and NSTCs (CD15⁻/CD133⁻) isolated from patient-derived GBM xenografts. The quantitative real-time-PCR (qRT-PCR) analyses demonstrated that only CD9, but not the other tetraspanins, was consistently upregulated in all tested GSCs relative to the matched NSTCs (Supplementary Figures S1a–d). Consistently, elevated expression of CD9 in GSCs relative to NSTCs was confirmed by immunofluorescent and immunoblot analyses of CD9 in CD133⁺/CD15⁺ GSCs and their matched CD133⁻/CD15⁻ NSTCs isolated from human GBMs or GBM xenografts (Figure 1b, Supplementary Figures S1e and f). To interrogate the correlation of CD9 and the established GSC markers SOX2 (SRY-related HMG-Box gene 2), OLIG2 (oligodendrocyte lineage transcription factor 2) and CD133, we performed immunofluorescent analyses and identified the co-enrichment of CD9 with these GSC markers in GSC-derived tumorspheres (Figure 1c and Supplementary Figure S1g). Flow cytometry analyses also confirmed that CD9 partially overlapped with the established GSC markers CD15, CD133, cell surface glycoprotein CD44 (CD44) and integrin $\alpha 6$ in glioma cells isolated from patient-derived GBM xenografts (Supplementary Figures S1h–o). As GSC population decreased during the serum-induced differentiation, we examined the expression of CD9 during GSC differentiation. A gradual decline of CD9 and the GSC marker SOX2 was observed during the serum-induced GSC differentiation, which was accompanied by the increase of the neuronal marker microtubule associated protein 2 (MAP2), indicating that CD9 expression was closely associated with GSC status (Figure 1d). These data demonstrate that tetraspanin CD9 is preferentially expressed in GSCs in human GBMs and may represent a new GSC marker.

CD9 is essential for the self-renewal and proliferation of GSCs. Because CD9 is preferentially expressed in GSCs relative to NSTCs, we next interrogated the functional significance of CD9 in the GSC maintenance by disrupting CD9 with short hairpin RNA (shRNA). The expressions of endogenous CD9 in D456 and T4121 GSCs were disrupted by two independent CD9 shRNAs (shCD9-1 and shCD9-2) as confirmed by immunoblot analyses and flow cytometry analyses (Supplementary Figures S2a and b). The *in vitro* limiting dilution assay demonstrated that silencing CD9 expression significantly inhibited GSC self-renewal, as demonstrated by the reduced primary tumorspheres and secondary tumorspheres derived from GSCs expressing shCD9 relative to those expressing shNT (Figure 1e, Supplementary Figure S2c and Supplementary Table S1). Consistently, the tumorsphere formation ability of GSCs was also impaired by CD9 disruption, resulting in the reduced tumorsphere numbers and sizes in the GSCs expressing shCD9 (Supplementary Figures S2d–f). We also examined

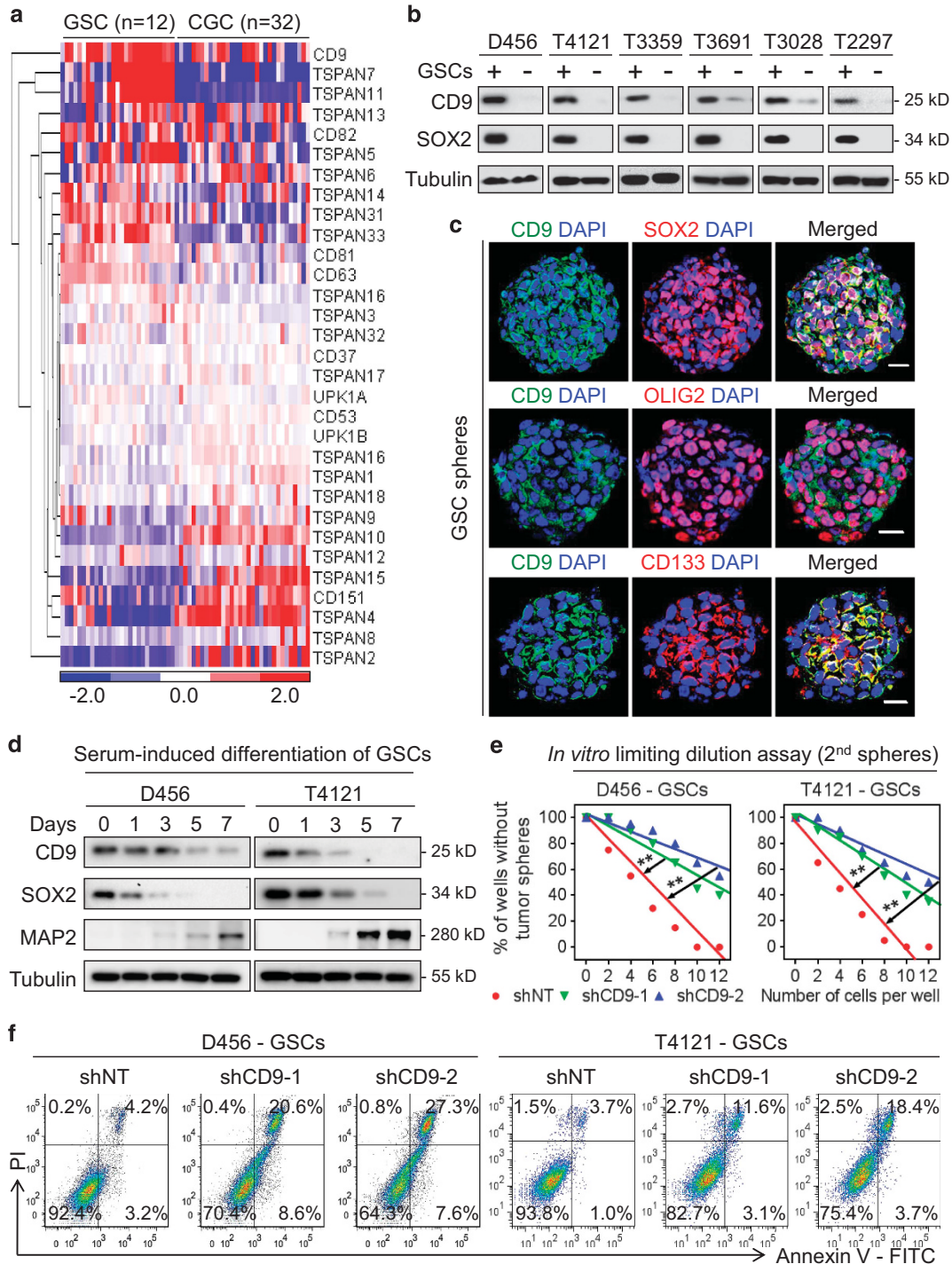


Figure 1 Tetraspanin CD9 is preferentially expressed in GSCs and is essential for the GSC maintenance. (a) The expression heatmap of tetraspanins in GSC lines ($n=12$) relative to CGCs ($n=32$) from the GEO profiles (GEO: GDS3885). Four candidates, including *CD9*, *TSPAN7*, *TSPAN11* and *TSPAN33* were significantly upregulated in GSCs relative to CGCs. Data were visualized using Cluster/Java Treeview. (b) Immunoblot analysis showing the preferential expressions of CD9 and the GSC marker SOX2 in GSCs ($n=6$) relative to the matched NSTCs ($n=6$) isolated from human GBMs. (c) Immunofluorescent staining of CD9 (in green) and the GSC marker SOX2 (in red, upper panel), OLIG2 (in red, middle panel) or CD133 (in red, lower panel) in GSC tumorspheres. Scale bar represents 25 μm . (d) Immunoblot analyses of CD9, the GSC marker SOX2 and the neuronal differentiation marker MAP2 during the serum-induced differentiation of GSCs. The levels of CD9 and the GSC marker SOX2 decreased, while the expression of the differentiation marker MAP2 concomitantly increased over a 7-day period. (e) *In vitro* limiting dilution analyses of the secondary tumorsphere formations of GSCs expressing shCD9 (shCD9-1 and -2) or non-targeting shRNA (shNT, control). Disrupting CD9 expression attenuated the self-renewal capacity of GSCs. $**P < 0.01$. (f) Representative FACS analysis of cell apoptosis in GSCs expressing shCD9 and shNT. FITC-conjugated Annexin V and PI were used as the early stage and late stage apoptotic marker, respectively. Silencing CD9 in GSCs induced apoptotic cell death. Experiments were repeated independently for three times (b–f). $**P < 0.01$

the impact of CD9 disruption on GSC differentiation. GSCs expressing shCD9 or shNT were cultured in serum-induced differentiation medium for 5 days. Immunoblot analyses showed that the levels of astrocytic marker glial fibrillary acidic protein (GFAP) and neuronal marker MAP2 were significantly elevated in glioma cells expressing shCD9 relative to the control cells expressing shNT (Supplementary Figure S2g). These results indicate that CD9 disruption could accelerate GSC differentiation. As CD9 has been demonstrated to regulate tumor cell viability,^{26,27} we investigated the impact of CD9 on GSC proliferation and apoptosis, and found that CD9 disruption apparently inhibited GSC proliferation and significantly induced GSC apoptosis (Supplementary Figure S2h and Figure 1f). Collectively, these data demonstrate that CD9 is essential for maintaining the self-renewal and proliferation of GSCs.

CD9 interacts with gp130 to mediate its function in GSCs. Tetraspanins have been reported to function through interaction with other membrane proteins, including cytokine receptors, to regulate the downstream signaling transduction,^{12,28} whereas the CD9-binding partner on cell surface of GSCs has not been defined. To identify the CD9-interacting proteins in GSCs, we transduced GSCs with a Flag-tagged CD9, and the CD9 associated protein complex was then immunoprecipitated with anti-Flag antibody followed by MS analyses. To this end, we identified gp130, a transmembrane IL-6 receptor subunit that regulates the activation of STAT3 signaling, as the top candidate of CD9-interacting proteins on cell surface (Figure 2a and Supplementary Table S2). The interaction between CD9 and gp130 was confirmed by the co-immunoprecipitation assay, as gp130 protein was detected in the anti-CD9-Flag immunoprecipitated protein complex and *vice versa* (Figure 2b and Supplementary Figure S3a). Furthermore, immunofluorescent analyses validated the co-localization of CD9 and gp130 in GSC populations (D456 and T4121) (Figure 2c and d). These data suggest that CD9 could be functionally associated with gp130 in regulating the GSC phenotype. To address the role of gp130 on GSC viability and self-renewal property, we used specific shRNAs against gp130 to disrupt endogenous gp130 expression in GSCs, and confirmed the effective disruption of gp130 by immunoblot analyses (Figure 2e and Supplementary Figure S3b). The cell proliferation analyses demonstrated that silencing gp130 expression potently inhibited GSC growth (Figure 2f). Moreover, the self-renewal of GSCs was significantly impaired by gp130 disruption, as demonstrated by the reduced tumorspheres derived from GSCs expressing shgp130 relative to those expressing shNT (Figure 2g and Supplementary Table S3). In addition, gp130 disruption promoted GSC differentiation, as the levels of astrocytic marker GFAP and neuronal marker MAP2 were elevated in glioma cells expressing shgp130 relative to those expressing shNT (Supplementary Figure S3c). As CD9 binds to gp130 in GSCs, we next examined whether the binding of CD9 to gp130 could impact gp130 in GSCs. Immunoblot analyses showed that disrupting CD9 by shRNAs markedly reduced gp130 protein levels in GSCs (Figure 2h), indicating that CD9 may control GSC

maintenance through regulating gp130 protein stability in GSCs.

CD9 stabilizes gp130 by blocking its ubiquitin-dependent lysosomal degradation. As CD9 bound to gp130 and disrupting CD9 markedly reduced gp130 protein in GSCs, we next investigated how CD9 maintained gp130 protein in GSCs. The qRT-PCR results showed that the mRNA level of gp130 was not affected by CD9 disruption (Figures 3a and b), thus it is possible that CD9 regulated gp130 protein at the post-transcriptional level. As ubiquitin-dependent degradation affects gp130 stability in multiple normal and malignant cells,²⁹ we investigated whether CD9 stabilized gp130 by preventing its ubiquitin-dependent degradation in GSCs. The ubiquitination-dependent protein degradation may be mediated by either proteasome or lysosome.^{30,31} Although both pathways have been reported in the regulation of gp130,²⁹ only the lysosome inhibitor chloroquine (CHL), but not the proteasome inhibitor MG132, could significantly extend the turnover of gp130 protein in GSCs (Figures 3c, d, Supplementary Figures S4a and b), suggesting that the lysosome-mediated protein degradation is the dominant mechanism controlling gp130 protein stability in GSCs. The ubiquitination assay showed that CD9 disruption markedly increased poly-ubiquitination of gp130 protein in GSCs treated with lysosome inhibitor CHL (Figure 3e). Consistently, whereas disruption of CD9 reduced the gp130 protein level in GSCs, treatment of the lysosome inhibitor CHL partially restored gp130 protein level (Figures 3f and g), indicating that CD9 may prevent gp130 from the lysosome-mediated degradation. Taken together, our results indicate that CD9 stabilizes gp130 by coupling gp130 and preventing the ubiquitin-dependent lysosomal degradation of gp130 protein in GSCs.

CD9 is required for the gp130-mediated BMX-STAT3 signaling in GSCs. Because CD9 binds to gp130 and stabilizes gp130 protein in GSCs, we next investigated whether CD9 regulates the downstream signaling of gp130 in GSCs. Gp130-mediated signaling is crucial for the activation of STAT3 pathway in GSCs in response to multiple cytokines, including IL-6.²¹ We thus sought to determine the effect of CD9 disruption on the gp130-mediated IL-6-STAT3 pathway. Immunoblot analyses showed that IL-6 stimulation activated STAT3 pathway in GSCs, as represented by the elevated phosphorylations of the downstream signaling transducer BMX (p-Tyr40) and STAT3 (p-Tyr705) (Figures 4a and b). However, disrupting CD9 by shRNA reduced gp130 protein and potently attenuated the IL-6-activated activating phosphorylations of BMX and STAT3 in GSCs (Figures 4a and b). The association of CD9 expression and STAT3 activation was also confirmed in human GBMs, as demonstrated by positive correlation of CD9 level and p-STAT3 (p-Tyr705) level in human GBMs from TCGA database (Supplementary Figure S4c). Moreover, the expressions of STAT3 downstream effectors related to cell proliferation, including Bcl-xL and c-Myc were attenuated by CD9 disruption (Figures 4c and d). These data demonstrate that CD9 is required for the gp130-mediated BMX-STAT3 signaling in GSCs.

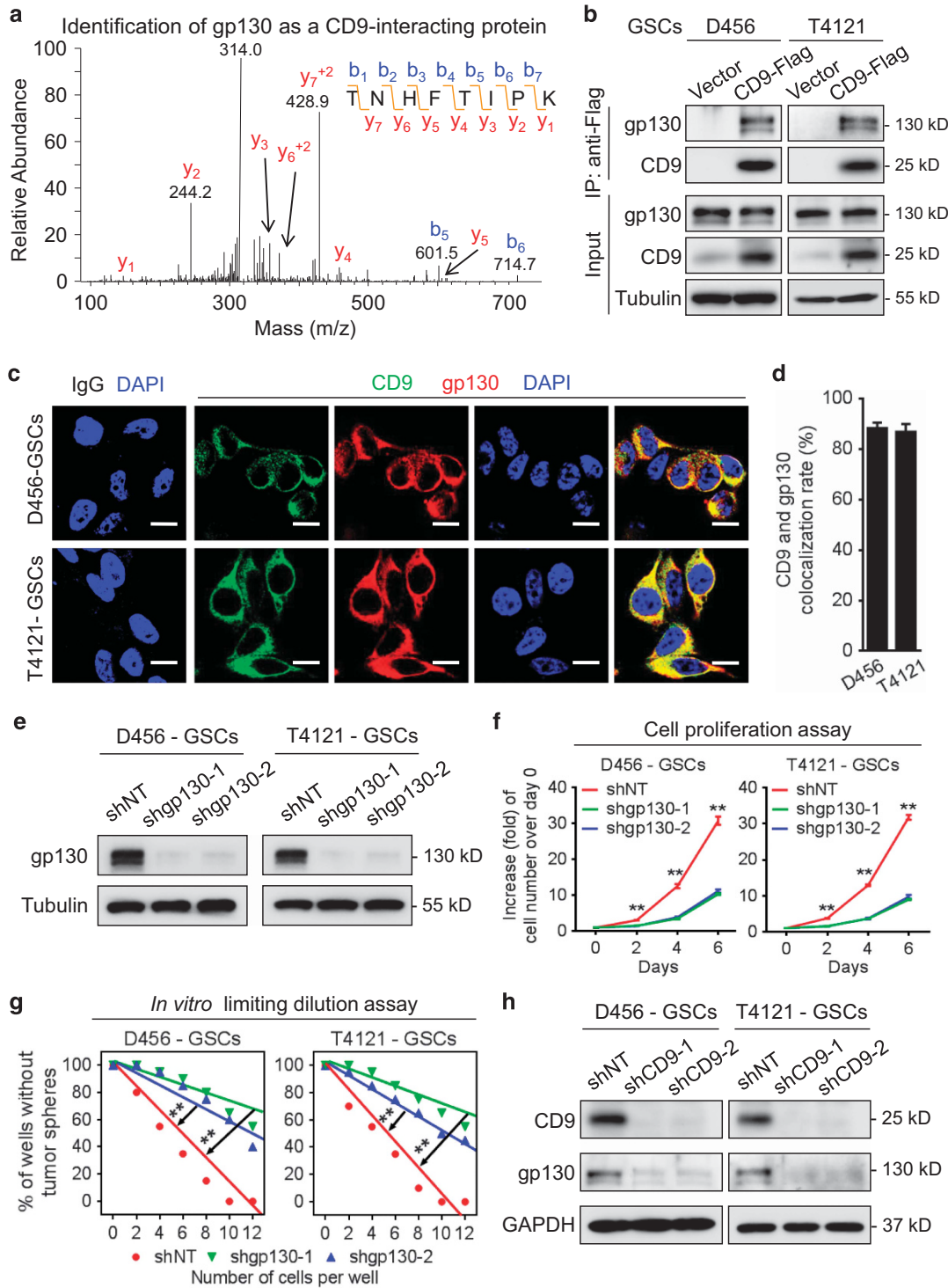


Figure 2 CD9 interacts with gp130 to mediate its function in GSCs. (a) MS analysis identified gp130 as the key interacting protein of CD9. CD9 was immunoprecipitated from T4121 GSCs expressing CD9-Flag using anti-Flag-conjugated beads. Gp130 was identified through MS analysis by peptides covering the gp130 protein sequence. A representative detected peptide (TNHFTIPK) of gp130 was shown. (b) Co-immunoprecipitation of gp130 with CD9 using anti-Flag-conjugated beads in D456 and T4121 GSCs transduced with CD9-Flag or vector control. (c) Representative immunofluorescent images of CD9 (in green) and gp130 (in red) in D456 and T4121 GSCs. Co-localization of CD9 and gp130 was detected in GSCs. Scale bar represents 10 μ m. (d) Quantification of co-localization rate of CD9 and gp130 in c. The co-localization rate of CD9 with gp130 was determined with five randomly selected images using Leica LAS AF Lite software. (e) Immunoblot analysis of gp130 in GSCs expressing shgp130 or shNT. Disrupting gp130 by shRNA effectively reduced gp130 expression. (f) Cell proliferation assay of GSCs expressing shgp130 or shNT. Gp130 disruption significantly suppressed GSC proliferation. $**P < 0.01$. (g) *In vitro* limiting dilution assay of GSCs expressing shgp130 or shNT. Disruption of gp130 markedly suppressed GSC self-renewal. $**P < 0.01$. (h) Immunoblot analyses of CD9 and gp130 in GSCs expressing shCD9 or shNT. Experiments were performed independently for three times (b–h). Data are shown as mean \pm S.D. (d, f). $**P < 0.01$

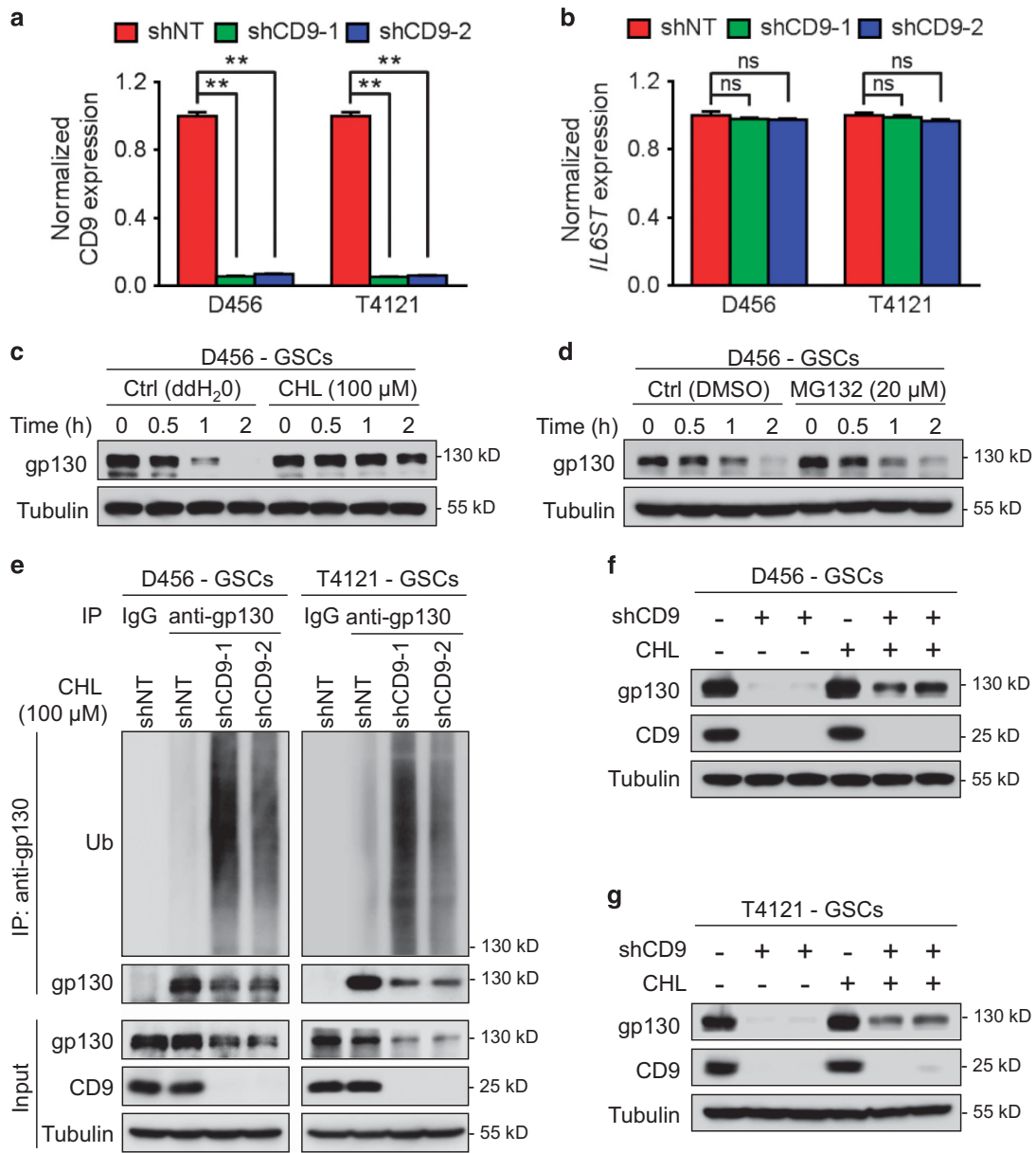


Figure 3 CD9 stabilizes gp130 by preventing the ubiquitin-dependent lysosomal degradation. (a, b) qRT-PCR analysis of *CD9* (a) and *IL6ST* (gene encoding for gp130) (b) in D456 and T4121 GSCs expressing shCD9 or shNT. Silencing CD9 did not affect mRNA level of gp130 in GSCs. $**P < 0.01$; NS, not significant. (c, d) Immunoblot analyses of gp130 in GSCs treated with lysosome inhibitor CHL (c) or proteasome inhibitor MG132 (d). T4121 GSCs were pretreated with CHL (100 μM) or MG132 (20 μM) or control vehicles for 1 h. At the beginning of the chase, cycloheximide (25 μg/ml) was added to each sample to block protein synthesis and cells were collected at indicated time points to examine the expression of gp130. The lysosome inhibitor, but not the proteasome inhibitor, extended the protein stability of gp130 in GSCs. (e) Ubiquitination assay showing that disrupting CD9 expression promoted gp130 ubiquitination and reduced gp130 protein in GSCs. D456 and T4121 GSCs expressing shCD9 or shNT were treated with lysosome inhibitor CHL (100 μM) for 14 h, and collected for immunoprecipitation of gp130 followed by immunoblot analyses of ubiquitin. Precipitation with normal rabbit IgG was used as negative controls. Total cell lysates (input) were also immunoblotted with antibodies against gp130, CD9 and tubulin. (f, g) Immunoblot analyses of gp130 in GSCs expressing shCD9 or shNT in combination with the treatment of lysosome inhibitor CHL or the vehicle control. CHL (100 μM) or the vehicle was added to D456-GSCs (f) or T4121-GSCs (g) expressing shCD9 or shNT. Cells were collected after 14 h for immunoblot assay of gp130, CD9 and tubulin. All experiments were performed independently for three times. Data are shown as mean ± S.E.M. (a, b). $**P < 0.01$; NS, not significant

To examine whether restored activity of STAT3 could compromise the suppressive effect of CD9 disruption, we transduced a Flag-tagged constitutively activated STAT3 (STAT3-C-Flag) into GSCs expressing shCD9 or shNT control (Figure 5a). Forced expression of STAT3-C rescued GSC

tumorsphere formation ability (Figures 5b–d) and the self-renewal capacity (Figure 5e and Supplementary Table S4) that were impaired by CD9 disruption. Consistently, ectopic expression of STAT3-C in the GSCs expressing shCD9 restored cell proliferation and reduced cell apoptosis relative

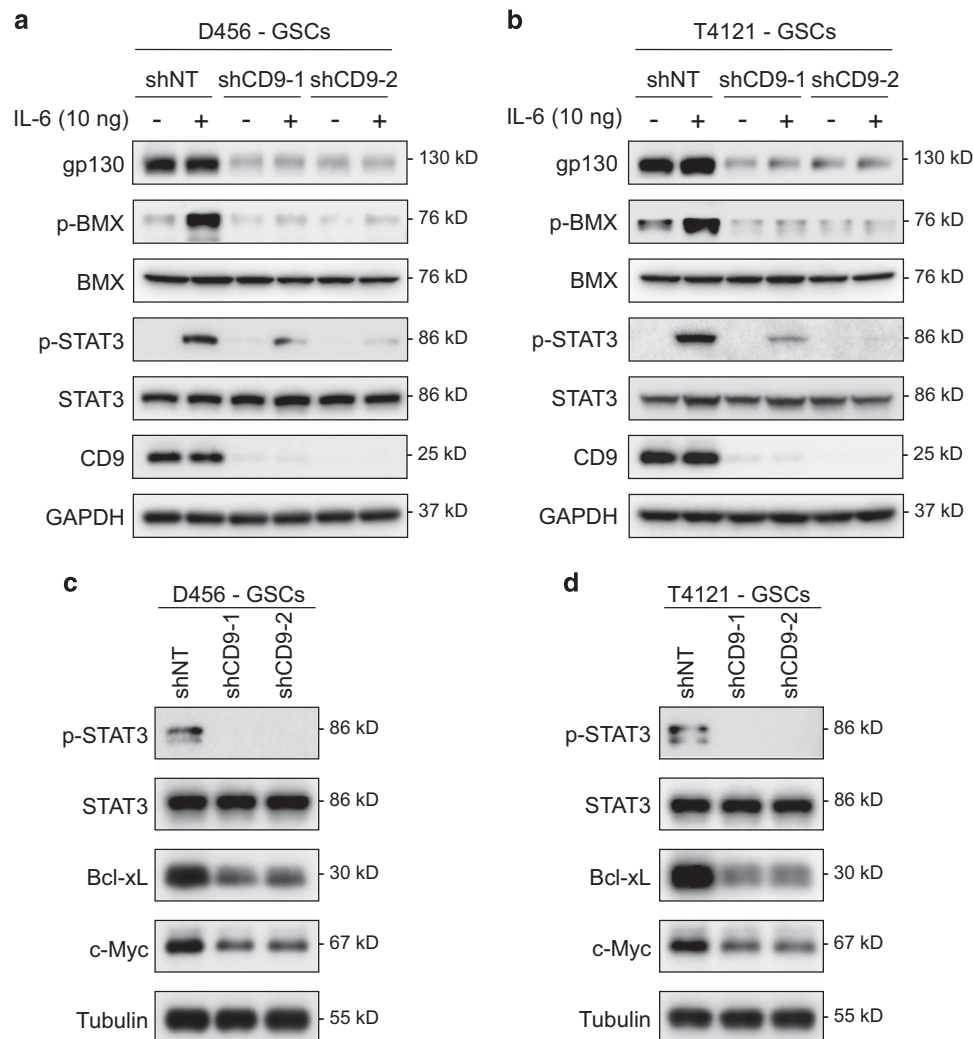


Figure 4 CD9 is required for the gp130-mediated BMX-STAT3 signaling in GSCs. (a, b) Immunoblot analyses of CD9, gp130, p-BMX (p-Tyr40), BMX, p-STAT3 (p-Tyr705) and STAT3 in D456-GSCs (a) or T4121-GSCs (b) expressing shCD9 or shNT in combination with IL-6 treatment. Cells were treated with IL-6 (10 ng/ml) or control vehicle for 10 min and were collected for immunoblot analyses. CD9 disruption abolished the IL-6 induced activating phosphorylations of BMX (p-Tyr40) and STAT3 (p-Tyr705). (c, d) Immunoblot analyses of p-STAT3 (p-Tyr705), STAT3, Bcl-xL and c-Myc in D456-GSCs (c) or T4121-GSCs (d) expressing shCD9 or shNT. Silencing CD9 attenuated the activity of STAT3 (p-STAT3) and thus suppressed the expressions of STAT3 downstream targets Bcl-xL and c-Myc. All experiments were performed independently for three times

to those expressing shCD9 only (Figures 5f and g), indicating that STAT3-C compromised the suppressive effect of CD9 disruption on GSC maintenance. Collectively, these data demonstrate that CD9 functions through mediating the gp130-STAT3 signaling axis to maintain the GSC phenotype.

CD9 promotes GSC-driven tumor propagation through the gp130-STAT3 signaling axis. Because STAT3 activation is crucial for GBM tumor progression and CD9 is required for the STAT3 signaling in GSCs, CD9 may have a critical role in maintaining GSC tumorigenic potential. To determine the functional significance of CD9 in GSC-driven tumor growth, T4121 or D456 GSCs expressing luciferase along with shCD9 or shNT were implanted into mouse brains to examine the impact of CD9 disruption on GSC tumor growth. The *in vivo* bioluminescent imaging showed that silencing CD9

expression markedly impaired GSC-driven intracranial tumor growth (Figures 6a, b, Supplementary Figures S5a and b). The retarded tumor sizes of the shCD9-expressing xenografts relative to the shNT-expressing xenografts were confirmed by H&E staining (Figure 6c). Consequently, the survivals of mice bearing the shCD9-expressing xenografts were significantly extended relative to those bearing the shNT-expressing xenografts (Figure 6d and Supplementary Figure S5c). Immunofluorescent analyses confirmed a significant reduction of CD9-positive tumor cells in the xenografts expressing shCD9 relative to the control xenografts (Supplementary Figures S5d and e). As activation of STAT3 signaling is required for GSC-driven tumor propagation, we examined the effect of CD9 disruption on the activating phosphorylation of STAT3 (p-Tyr705) in the GSC-derived xenografts. Immunohistochemical analyses showed

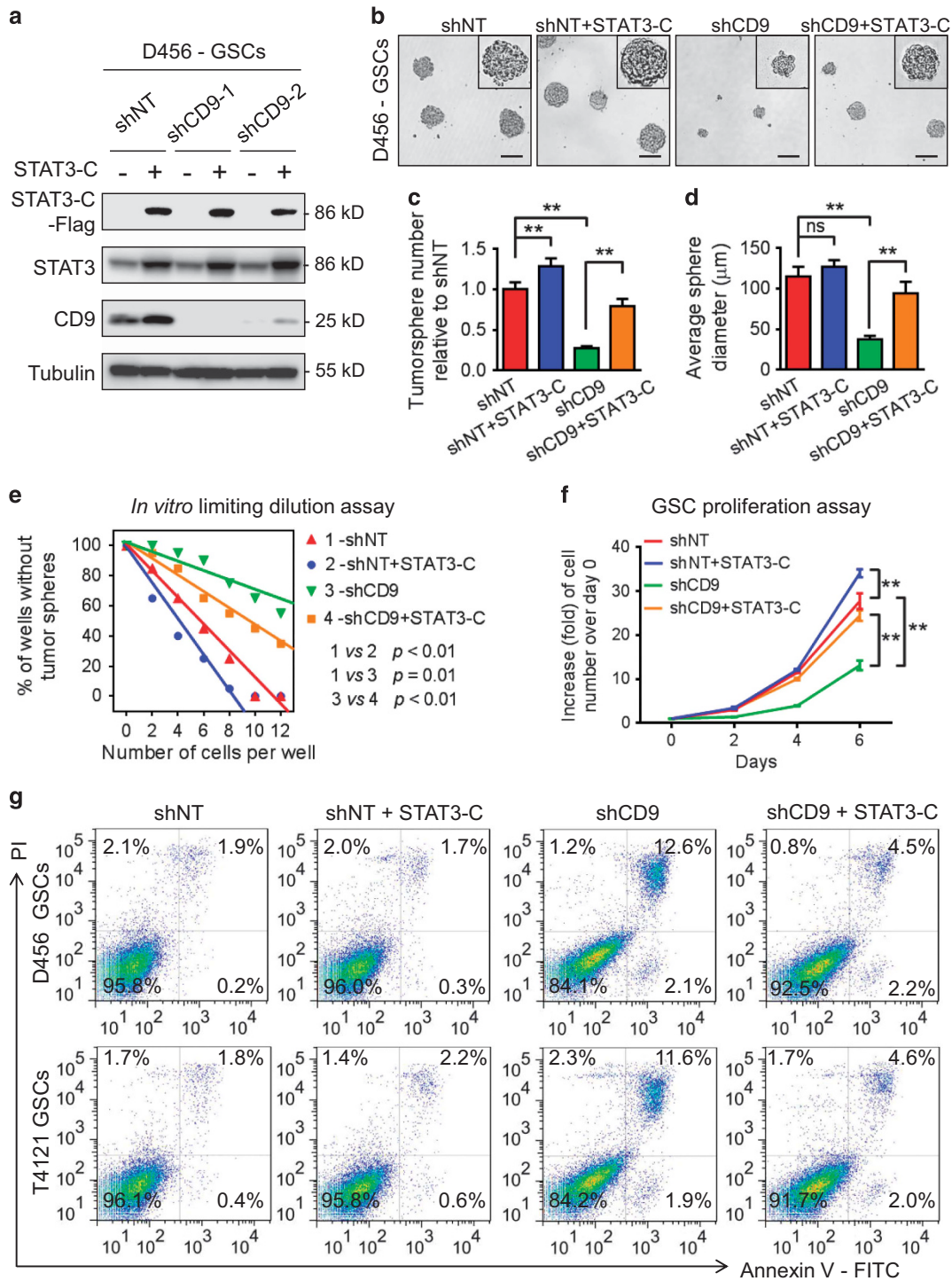


Figure 5 Expression of a STAT3-C compromises GSC maintenance impaired by CD9 disruption. (a) Immunoblot analyses of Flag-tagged STAT3-C, STAT3 and CD9 in D456 GSCs transduced with STAT3-C or vector and shCD9 or shNT control. (b–d) The representative images (b) and quantification of sphere numbers (c) and sphere diameters (d) of D456 GSCs expressing shCD9 and/or STAT3-C. Scale bar = 100 μm. STAT3-C compromised the inhibitory effect of CD9 disruption on GSC tumorsphere formation. ** $P < 0.01$; NS, not significant. (e) *In vitro* limiting dilution assay of GSCs expressing shCD9 and/or STAT3-C. Ectopic expression of STAT3-C rescued the GSC self-renewal capacity impaired by CD9 disruption. (f) Cell proliferation assay of GSCs expressing shCD9 and/or STAT3-C. STAT3-C restored GSC proliferation that was impaired by CD9 disruption. ** $P < 0.01$. (g) Representative FACS analyses of apoptotic cell death in GSCs expressing shCD9 and/or STAT3-C. Expression of STAT3-C partially rescued GSC apoptosis induced by CD9 disruption. FITC-conjugated Annexin V and PI were used as the early stage and late stage apoptotic marker, respectively. All experiments were performed independently for three times. Data are shown as mean \pm S.D. (c, d, f). ** $P < 0.01$; NS, not significant

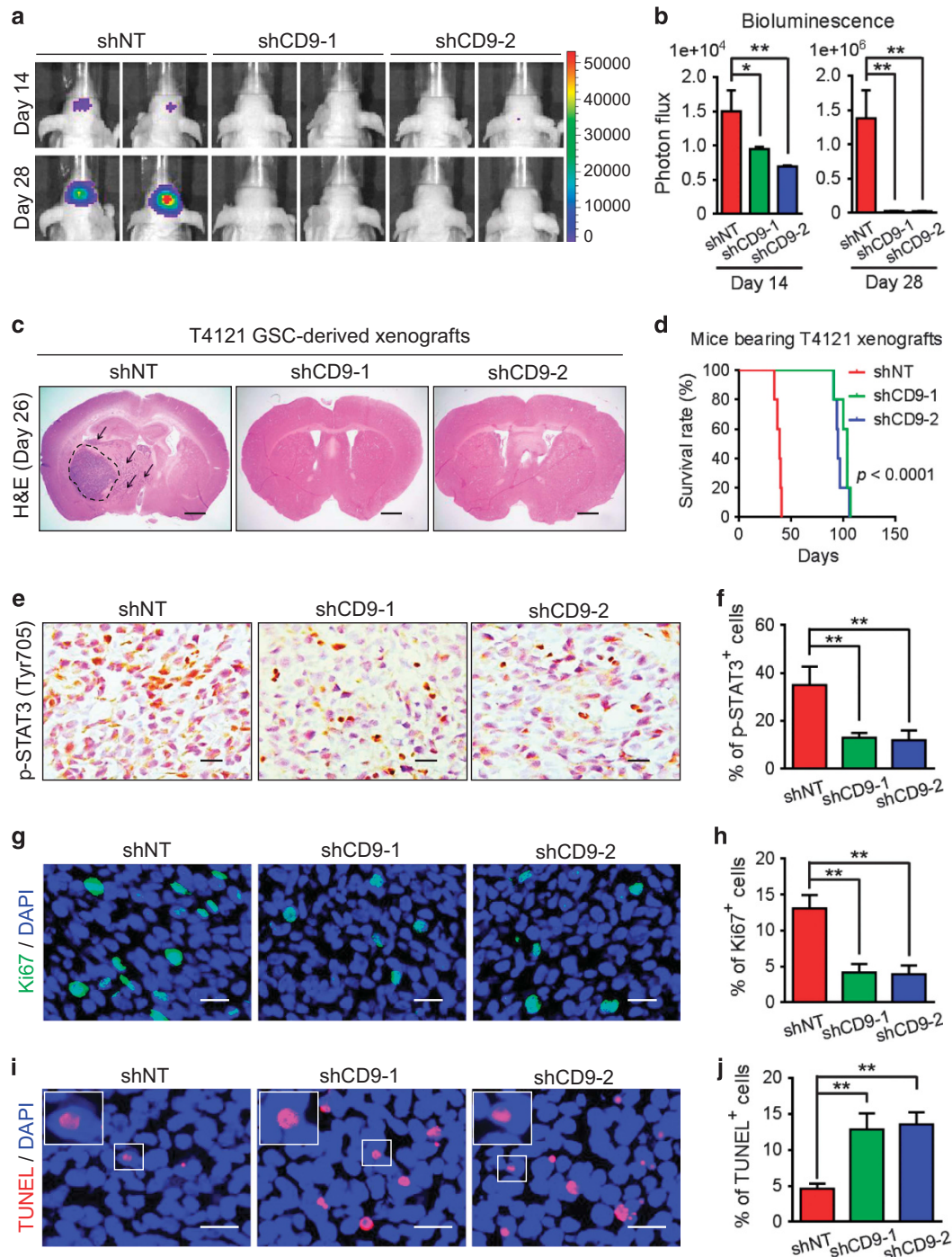


Figure 6 Disrupting CD9 inhibits GSC-driven tumor growth and STAT3 activation *in vivo*. **(a, b)** Representative bioluminescent images **(a)** and the quantification **(b)** of xenografts derived from T4121 GSCs expressing shCD9 or shNT at day 14 and day 28 after tumor implantation. Silencing CD9 markedly suppressed GSC-driven tumor growth. $*P < 0.05$; $**P < 0.01$ ($n = 5$ per group). **(c)** Hematoxylin and eosin (H&E) staining of cross sections of mouse brains bearing xenografts derived from T4121 GSCs expressing shCD9 or shNT. Xenografts were collected at day 26 after tumor implantation. The dashed line indicated the xenograft regions in mouse brain. Arrows indicated tumor infiltration into the surrounding normal tissue. Scale bar represents 1000 μm . **(d)** Kaplan–Meier survival analysis of mice bearing xenografts derived from T4121 GSCs expressing shCD9 or shNT. Disrupting CD9 significantly extended animal survival. $P < 0.0001$ ($n = 5$ per group). **(e, f)** Immunohistochemical staining of p-STAT3 (p-Tyr705, **e**) and the quantification of p-STAT3-positive cells **(f)** in xenografts derived from T4121 GSCs expressing shCD9 or shNT. Xenografts were collected at day 38 after tumor implantation. Scale bar represents 25 μm . $**P < 0.01$. **(g, h)** Immunofluorescent staining of Ki67 (in green, **g**) and the quantification of Ki67-positive cells **(h)** in xenografts derived from T4121 GSCs expressing shCD9 or shNT. Xenografts were collected at day 38 after tumor implantation. Scale bar represents 25 μm . $**P < 0.01$. **(i, j)** TUNEL staining detecting apoptosis (TUNEL, in red, **i**) and the quantification of the TUNEL-positive cells **(j)** in xenografts derived from T4121 GSCs expressing shCD9 or shNT. Silencing CD9 induced apoptotic cell death in GSC-derived tumors. Xenografts were collected at day 38 after tumor implantation. Scale bar represents 25 μm . $**P < 0.01$. Experiments were performed independently for three times **(e–j)** Data are shown as mean \pm S.E.M. **(b)** or mean \pm S.D. **(f, h, j)**. $*P < 0.05$; $**P < 0.01$

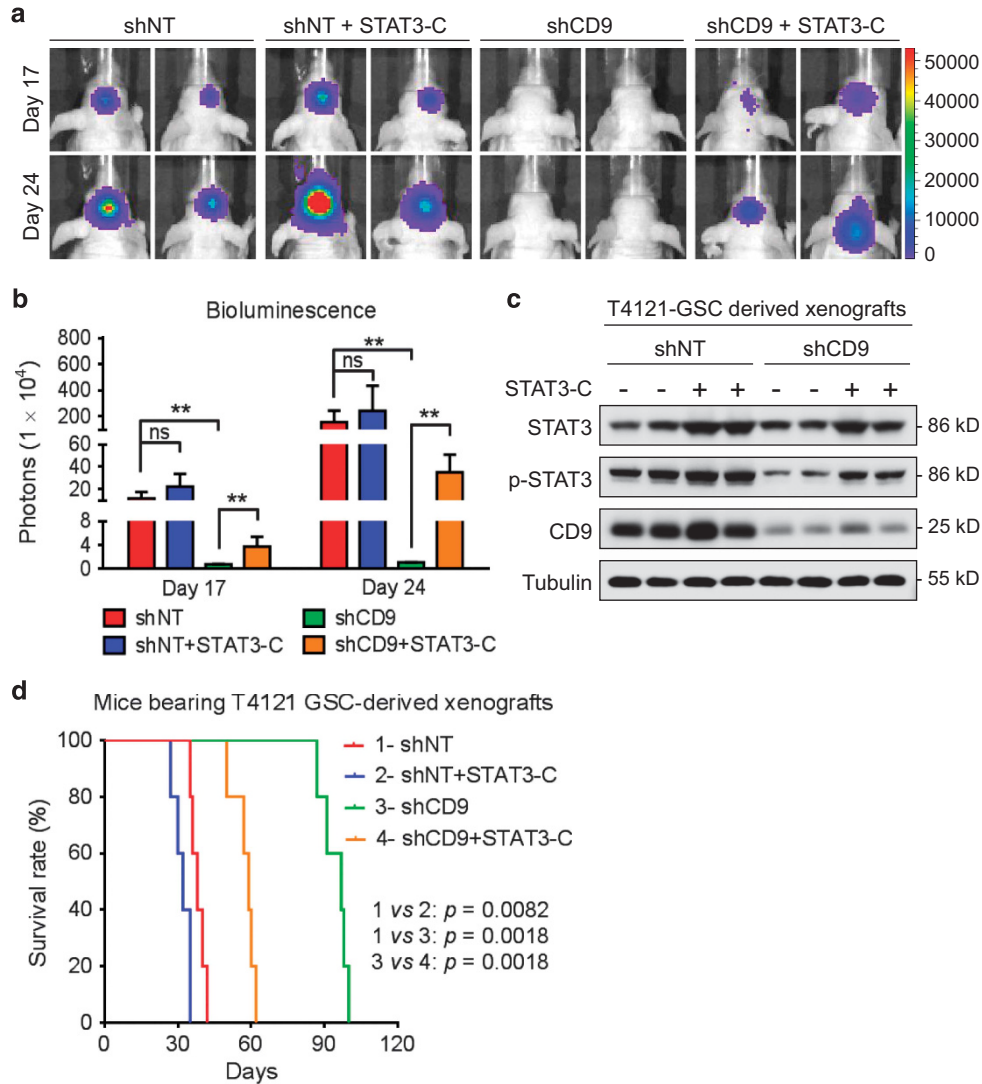


Figure 7 Expression of the STAT-C restores GSC-driven tumor propagation impaired by CD9 disruption. (a, b) Representative bioluminescent images (a) and the quantification (b) of xenografts derived from T4121 GSCs expressing shCD9 and/or STAT3-C at day 17 and day 24 after tumor implantation. Data are shown as mean \pm S.E.M. (b). $**P < 0.01$; NS, not significant. $n = 5$ per group. (c) Immunoblot analyses of STAT3, p-STAT3 and CD9 in xenografts derived from T4121 GSCs transduced with shCD9 and/or STAT3-C or control vectors. Enforced expression of STAT3-C rescued the level of p-STAT3 (p-Tyr705) in xenografts derived from GSCs expressing shCD9. Xenografts were collected at day 30 after tumor implantation. (d) Kaplan–Meier survival analysis of mice bearing xenografts derived from T4121 GSCs expressing shCD9 and/or STAT3-C. STAT3-C introduction attenuated the increased survival caused by CD9 disruption in GSCs. $n = 5$ per group. Experiments were performed independently for three times (c)

much fewer p-STAT3-positive tumor cells in the shCD9-expressing xenografts than the shNT-expressing xenografts (Figures 6e, f, Supplementary Figures S5f and g). Further analyses indicated that the xenografts derived from the shCD9-expressing GSCs contained much fewer Ki67-positive proliferative cells (Figures 6g and h) and much more TUNEL-positive apoptotic cells relative to the control tumors (Figures 6i and j), indicating that CD9 disruption significantly reduced tumor cell proliferation and promoted cell apoptosis *in vivo*. Taken together, these data demonstrate that CD9 is critical for maintaining STAT3 signaling *in vivo* to support GSC-driven tumor propagation.

As CD9 disruption inhibited STAT3 activation and suppressed GSC tumor propagation, we examined whether

ectopic expression of the STAT3-C could rescue the tumor growth impaired by CD9 disruption. GSCs expressing luciferase were transduced with STAT3-C along with shCD9 or shNT, and then implanted into mouse brains. Immunofluorescent analyses confirmed a significant reduction of CD9-positive tumor cells in the shCD9-expressing xenografts relative to the shNT-expressing xenografts (Supplementary Figures S6a and b). Bioluminescent analyses showed that expression of the STAT3-C markedly restored the tumor growth that was impaired by CD9 disruption (Figures 7a and b). Restored activation of p-STAT3 (p-Tyr705) was also detected in the xenografts expressing STAT3-C and shCD9 relative to the xenografts expressing shCD9 alone (Figure 7c). Consequently, the survivals of mice bearing the xenografts

expressing shCD9 plus STAT3-C were significantly reduced relative to those bearing the xenografts expressing shCD9 alone (Figure 7d). These results demonstrate that CD9 maintains GSC tumorigenic capacity through promoting STAT3 activation.

Discussion

GBM is the most common and lethal primary brain tumor that is highly resistant to current treatment.² GSCs are critical cancer cells that contribute to malignant progression, therapeutic resistance and tumor recurrence in GBM.^{5,32} As STAT3 signaling is commonly activated in GSCs, and the BMX-mediated STAT3 activation is required for maintaining the self-renewal and tumorigenic potential of GSCs,^{21,22,23} disrupting STAT3 signaling pathway may potentially disrupt GSCs and have therapeutic potential. However, targeting STAT3 transcription factor itself is not clinically achievable, as STAT3 is required for other functions in normal cells.^{20,22} Thus, identification of unique upstream regulators controlling STAT3 activation in GSCs may offer new therapeutic targets for developing GSC-specific therapeutics to improve GBM treatment. In this study, we identify tetraspanin CD9 to be preferentially expressed in GSCs and demonstrate that CD9 is crucial for maintaining STAT3 activation in GSCs. We uncover that CD9 functions through stabilizing the IL-6 receptor subunit gp130, which in turn promotes the BMX-mediated activating phosphorylation of STAT3. Specifically, CD9 couples gp130 to block the ubiquitin-dependent lysosomal degradation of gp130 and promotes the gp130-BMX-STAT3 signaling in GSCs (Figure 8). Thus, tetraspanin CD9 functions as a key molecular organizer for the pro-survival STAT3 signaling in GSCs. As targeting CD9 potentially inhibited GSC tumorsphere formation, cell proliferation and tumor growth, and CD9 is a cell surface protein preferentially and commonly expressed in GSCs, CD9 represents a unique molecular target for developing specific therapeutics against GSCs. In addition, as CD9 expression positively correlates with glioma tumor grades and predicts poor prognosis of GBM patients (Supplementary Figure S7), CD9 can also serve as a useful marker for diagnostic and prognostic determination of GBM.

CD9 functions through regulating gp130 protein stability to maintain the self-renewal and tumorigenic potential of GSCs. Gp130 is a glycoprotein that mediates the activation of key pro-survival pathways crucial for tumor cell proliferation, invasion and angiogenesis.^{21,33,34} Amplification of gp130 gene and the abnormal stabilization of the gp130 protein have been shown to be closely associated with tumor progression.^{33,34} The protein level of gp130 in normal cells is tightly regulated at the post-translational level by the ubiquitin-dependent degradation, endocytosis and caspase-induced proteolysis.^{29,35,36} It is highly possible that the abnormally elevated gp130 protein level in tumor cells may be caused by dysregulated post-translational processes. Our results showed that CD9 coupled gp130 to reduce gp130 ubiquitination, thereby sustaining high level of gp130 in GSCs for maintaining STAT3 activation. As the ubiquitin-dependent degradation of gp130 in normal cells has been shown to be mediated by the E3 ligase Cbl when triggered by the IL-6,²⁹ we

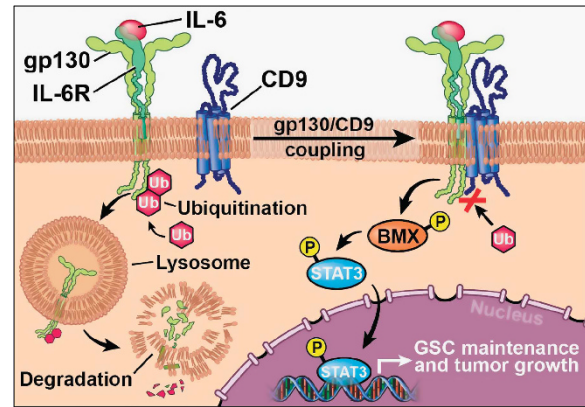


Figure 8 A schematic diagram shows that CD9 binds to gp130 and stabilizes gp130 by blocking its ubiquitin-dependent lysosomal degradation to promote the BMX-mediated STAT3 activation in GSCs. The binding of CD9 to gp130 prevents gp130 from ubiquitination and lysosomal degradation, thus facilitates the signal transduction of the IL-6-gp130-BMX-STAT3 signaling pathway in GSCs to maintain GSC self-renewal and tumorigenic potential

speculate that CD9 coupling gp130 may block the Cbl binding on gp130 to prevent its ubiquitination and lysosomal degradation in GSCs and our preliminary data support this hypothesis (Supplementary Figure S8). Of note, although multiple post-translational processes participate in the regulation of gp130 stability, it seems that lysosomal degradation is the dominant mechanism controlling gp130 level in GSCs, because the lysosome inhibitor CHL but not the proteasome inhibitor MG132 could potentially restore the gp130 protein level in GSCs (Figures 3c, d, Supplementary Figures S4a and b). In addition, gp130 can be activated by ligands such as IL-6 or leukemia inhibitory factor (LIF), and is crucial for signal transductions in multiple stem cells, including ES and cancer stem cells.^{37–39} In GSCs, gp130 is critical for the maintenance of the stem cell-like phenotype of GSCs (Figures 2f and g). As our study demonstrated that CD9 stabilized gp130 expression, we speculate that CD9 could also affect LIF-stimulated gp130 downstream signal transduction, which warrants further investigation.

The activation of STAT3 pathway is a key downstream signaling event of gp130. STAT3 signaling has been shown to be crucial for the maintenance of the stem cell property in ES, somatic stem cells and cancer stem cells, including GSCs.^{22,40,41} As STAT3 has essential roles in several cellular activities in normal cells and STAT3 is a transcription factor, direct targeting of STAT3 may cause collateral damage on normal cells, including somatic stem cells.^{22,40,41} Our study demonstrated that disrupting CD9 markedly reduced gp130 protein thus inhibited the activation of STAT3 in GSCs. Disrupting CD9 potentially suppressed GSC tumor growth, indicating that CD9 is an attractive therapeutic target to halt STAT3 signaling in GSCs to diminish their tumorigenic potential. Because CD9 is preferentially expressed in GSCs, but it is rarely expressed in neural stem cells or other normal brain cells,¹⁵ targeting CD9 may specifically disrupt GSC-driven tumor progression with minimal impact on the physiological function of brain. As a cell surface protein, the

tumor-supportive functions of CD9 have been reported to be neutralized by antibody blockade.¹⁴ Thus, CD9 may represent a potential therapeutic target to improve GBM treatment and overcome therapeutic resistance. In conclusion, this study revealed that CD9 stabilizes gp130 protein by blocking its lysosomal degradation to promote STAT3 signaling and support GSC tumor propagation and malignant progression. Targeting CD9 to interrupt the gp130-STAT3 signaling axis may have therapeutic potential to improve GBM treatment.

Materials and Methods

Isolation and culture of glioma cells. GSCs and matched NSTCs were isolated from GBM surgical specimens or patient-derived GBM xenografts using Papain Dissociation System as previously reported.^{3,7,8,22,42} T4121 xenograft was derived from an adult GBM tumor (WHO grade IV),²² and D456 (D456-MG) xenograft was derived from a pediatric GBM.⁴³ To isolate total glioma cells from GBM tumors, subcutaneous xenografts were collected and cut into small pieces and then were isolated using the Papain Dissociation System (Worthington Biochemical, Lakewood, NJ, USA) according to the manufacturer's instructions. The xenografts were further mechanically dissociated and the suspension was filtered with a 70 μ m cell strainer (BD Biosciences, San Jose, CA, USA) to remove tissue pieces in the xenografts. Cells were then cultured in Neurobasal medium (Invitrogen, Carlsbad, CA, USA) with B27 supplement and growth factors for 6 h to recover surface antigens, then passed through a 30 μ m nylon mesh to obtain a single-cell suspension. Human tumor cells were separated from host cells by using a Mouse Cell Depletion Kit (Miltenyi, 130-104-694, San Diego, CA, USA) according to the manufacturer's instructions. To sort GSCs and matched NSTCs, glioma cells were then labeled with the PE-conjugated anti-CD15 (130091375, Miltenyi) and the APC-conjugated anti-CD133 (130090854, Miltenyi) at 4 °C for 40 min followed by fluorescence-activated cell sorting to isolate the GSCs (CD15⁺/CD133⁺) and NSTCs (CD15⁻/CD133⁻). The cancer stem cell property of GSCs was confirmed by functional analyses (including *in vitro* limiting dilution assay, cell differentiation assay and *in vivo* tumorigenic assay) to assess the self-renewal potential, multi-lineage differentiation potency and *in vivo* tumor formation capacity of GSCs as described previously.^{3,7,8,22,42} Preferential expressions of GSC markers SOX2, OLIG2, L1CAM, CD15 and CD133 in GSC populations were validated. The enriched GSCs were constantly maintained as GBM xenografts and were only dissociated, sorted and cultured *in vitro* for functional experiments. GSCs cultured *in vitro* were maintained in Neurobasal medium (Invitrogen) with EGF (20 ng/ml, PeproTech, Rocky Hill, NJ, USA), bFGF (20 ng/ml, PeproTech) and B27 Supplement (20 μ l/ml, Life Technologies, Carlsbad, CA, USA). All GBM cells used in this study have been authenticated by STR analysis or karyotype analysis and were verified to be mycoplasma-free. All procedures were performed with informed consents approved by the institutional ethics committee of Cleveland Clinic and Southwest Hospital, and were in accordance with the principles of the WMA Helsinki Declaration and the Department of Health and Human Services Belmont Report.

Microarray analysis using GEO database. Microarray data of GEO (GEO: GDS3885) were applied to determine the expressions of tetraspanins in 12 cases of GSC lines and 32 cases of CGCs.²⁵ Gene cluster analyses were performed and visualized using Cluster/Java Treeview (<http://bonsai.hgc.jp/~mdehoon/software/cluster/software.htm>). Genes enriched in GSCs were identified when the ratio of average target expression in GSCs to CGCs was of statistical significance ($P < 0.05$).

Microarray analyses of CD9 from the Rembrandt database and TCGA database. Correlation of CD9 expression and glioma tumor grades was analyzed using the Rembrandt database (<https://gdoc.georgetown.edu/gdoc/workflows/translationalResearch>) and TCGA database (<https://tcga-data.nci.nih.gov/tcga>). The expressions of CD9 and p-STAT3 (p-Tyr705) in human GBMs and patient survival information were obtained from gene profiling data (Affymetrix U133A platforms) and protein expression data (MDA_RPPA_Core) from TCGA database.

Co-immunoprecipitation and MS analyses. For co-immunoprecipitation analyses of the CD9-binding proteins, GSC-transduced CD9-Flag or control vector were lysed on ice for 20 min in 20 mM Tris-HCl, pH 7.4, 150 mM NaCl, 5 mM EDTA,

10% glycerol, 1% CHAPS, 1 mM PMSF, 1 mM sodium fluoride, 1 mM sodium orthovanadate and a protease inhibitor cocktail (Roche, Pleasanton, CA, USA). The supernatant proteins were incubated with 15 μ l of anti-Flag M2 Affinity Gel (A2220, Sigma, St. Louis, MO, USA) for 14 h at 4 °C with constant rotation. Protein complexes were washed three times with 0.1% Triton X-100 in PBS and were competitively eluted with the Flag peptide (Sigma). To detect the binding of gp130 with CD9 or Cbl, the indicated GSCs were lysed and the supernatant proteins were incubated with 10 μ l of anti-gp130 antibody (06-291, Millipore, Billerica, MA, USA) or 5 μ l of isotype IgG (SC-2027, Santa Cruz, Santa Cruz, CA, USA) together with 20 μ l of Protein A/G PLUS-Agarose (SC-2003, Santa Cruz) for 14 h at 4 °C with constant rotation. Protein complexes captured by agarose beads were washed for three times with 0.1% Triton X-100 in PBS and eluted by boiling in Laemmli buffer. Samples were subjected to SDS-PAGE followed by silver staining or immunoblot analysis. For the liquid chromatography-MS analysis, the gel pieces with CD9 immunoprecipitated complex or control were dehydrated in acetonitrile, dried in a speed vacuum and digested with trypsin. The peptides were extracted from the polyacrylamide and were evaporated for MS analysis using LTQ-Orbitrap Elite Mass Spectrometer System (Thermo Scientific, Waltham, MA, USA). The data were analyzed by using all CID spectra collected in the experiment to search against the human reference sequence database with the program Sequest, which was integrated in Proteome Discoverer V1.4. (Thermo Scientific).

Immunoblot analyses. Immunoblot analyses were performed as previously described.^{9,44} The primary antibodies used in this study include the following: anti-CD9 (sc-13118, 1:1000, Santa Cruz); anti-gp130 (sc-655, 1:1000, Santa Cruz); anti-c-Myc (sc-40, 1:1000, Santa Cruz); anti-Cbl (sc-1651, 1:500, Santa Cruz); anti-STAT3 (p-Tyr705, #9131, 1:1000, Cell Signaling, Danvers, MA, USA); anti-STAT3 (#9139, 1:2000, Cell Signaling); anti-Bcl-xL (#2764, 1:500, Cell Signaling); anti-p-BMX (p-Tyr40, #3211, 1:1000, Cell Signaling); anti-BMX (ab59360, 1:1000, Abcam, Cambridge, UK); anti-Ubiquitin (646301, 1:500, Biologend, San Diego, CA, USA); anti-GFAP (644702, 1:1000, Biologend); anti-MAP2 (SMI-52 R, 1:1000, Covance, Princeton, NJ, USA); anti-Flag (637301, 1:1000, Biologend); anti-GAPDH (#2118, 1:5000, Cell Signaling); and anti-tubulin (T9026, 1:10 000, Sigma).

Ubiquitination assay. Ubiquitination assay was performed as previously described.^{9,45} D456 and T4121 GSCs expressing shCD9 or shNT were treated with lysosome inhibitor CHL (100 μ M) for 14 h, and collected for co-immunoprecipitation with anti-gp130 antibody (Millipore) followed by immunoblot analyses of ubiquitin. Precipitation with normal rabbit IgG was used as negative controls. Total cell lysates (input) were also immunoblotted with antibodies against gp130 (sc-655, 1:1000, Santa Cruz), CD9 (sc-13118, 1:1000, Santa Cruz) and tubulin (T9026, 1:10 000, Sigma).

Immunofluorescent staining and terminal dUTP nick end labeling staining. Immunofluorescent staining was performed as previously described using frozen human GBM specimens or GBM xenografts.^{9,42} Primary antibodies used in this study include the following: anti-CD9 (sc-13118, Santa Cruz); FITC-conjugated anti-human CD9 (555371, BD Biosciences); anti-gp130 (sc-655, Santa Cruz); anti-SOX2 (sc-17320, Santa Cruz); anti-OLIG2 (MABN50, Millipore); anti-CD133 (PAB12663, Abnova, Walnut, CA, USA); and anti-Ki67 (9615580, Abcam). Terminal deoxynucleotidyl transferase dUTP nick end labeling (TUNEL) staining was performed using an Apo-BrdU-Red *In Situ* DNA Fragmentation Assay Kit (Biovision, Milpitas, CA, USA) according to the manufacturer's instructions. Images were captured using an AMG EVOS FL microscope (Thermo Scientific, Waltham, MA, USA) or a Leica SP5 spectral confocal microscope (Leica, Buffalo Grove, IL, USA). The co-localization rate of CD9 and SOX2, OLIG2 or gp130 in cultured GSCs was determined with three or five randomly selected images using Leica LAS AF Lite software (Leica, Buffalo Grove, IL, USA). The percentage of CD9⁺, Ki67⁺ and TUNEL⁺ cells in GBM xenografts was determined using Image J software (National Institutes of Health, Bethesda, MD, USA) under five randomly selected microscopic fields at $\times 400$.

Immunohistochemical staining. Immunohistochemical staining of p-STAT3 (p-Tyr705) in GBM xenografts was performed using Dako REAL EnVision Detection System and the anti-p-STAT3 antibody (p-Tyr705, #9145, Cell Signaling) according to the manufacturer's protocol (DAKO, Carpinteria, CA, USA). The images were obtained under a Leica DM4000B microscope equipped with a QImaging EXi Aqua camera (QImaging, Surrey, BC, Canada). The percentage of p-STAT3⁺ cells was quantified in five randomly selected microscopic areas using Image J software.

In vitro limiting dilution assay. GSCs were implanted into a 96-well plate at a density of 0, 2, 4, 6, 8, 10 or 12 cells/well with 20 replicates for each concentration. Seven days after implantation, the numbers of tumorspheres in each well were determined and the sphere formation efficiency was calculated using extreme limiting dilution analysis as mentioned previously⁴⁶ (<http://bioinf.wehi.edu.au/software/elda/>).

Cell apoptosis assay. For cell apoptosis assay, GSCs expressing shCD9, shNT and/or STAT3-C were used to determine apoptotic cell death using the Annexin V-FITC Apoptosis Detection Kit (BD Pharmingen) according to the manufacturer's guidance. Signals of FITC-conjugated Annexin V and PI were detected using a BD LSR II flow cytometer. Data were analyzed and presented using FlowJo software (Tree Star).

Cell proliferation assay and tumorsphere formation assay. For cell proliferation assay, GSCs expressing shCD9, shgp130, shNT and/or STAT3-C were seeded in 96-well plates (1000 cells per well). The cell viability was determined at the 0, 2, 4 and 6 days after cell seeding using Cell Titer-Glo Luminescent Cell Viability Assay kit (Promega, Madison, WI, USA) following the manufacturer's protocol. For tumorsphere formation assay, GSCs expressing shCD9, shgp130, shNT and/or STAT3-C were plated in 96-well plates at a density of 1000 cells/well and cultured in Neurobasal medium with B27 Supplement and growth factors. Tumorsphere numbers and sizes were calculated at the seventh day after implantation as previously described.^{22,47}

GSC differentiation assay. GSCs were induced to differentiate by withdrawing growth factors and adding serum to cell culture medium as previously described.^{22,47} Briefly, GSCs expressing shCD9, shgp130 or shNT were cultured in DMEM with 10% FBS and were collected to examine the expressions of CD9, the GSC marker SOX2, the astrocytic marker GFAP, or the neural marker MAP2 using immunoblot assay.

Flow cytometry analyses. Mouse FITC-conjugated anti-human CD9 (555371, BD Biosciences, San Jose, CA, USA) and isotype Mouse IgG1 κ (555748, BD Biosciences) were used to determine the percentage of CD9-positive cells in GSCs expressing shCD9 and shNT. The above-mentioned CD9 flow antibody and PE-conjugated anti-CD15 (130091375, Miltenyi), APC-conjugated anti-CD133 (130090854, Miltenyi), APC-conjugated anti-CD44 (130098110, Miltenyi), APC-conjugated anti-Integrin α 6 (130097250, Miltenyi) or the corresponding isotype controls were used to determine the correlation between CD9, CD15, CD133 and CD44 or Integrin α 6. Cells were subjected to flow cytometry analyses using a BD LSR II flow cytometer. Data were analyzed and presented using FlowJo software (Tree Star, Ashland, OR, USA).

Lentiviral vectors construction. CD9-shRNA and gp130-shRNA lentiviral vectors and a non-targeting control shRNA (shNT, SHC002) vector were purchased from Sigma. The sequences of the shRNAs are listed in Supplementary Table S5. Lentiviral plasmids expressing Flag-tagged CD9 or Flag-tagged STAT3-C were constructed by cloning CD9-Flag or STAT3-C-Flag into a pCDH-MCS-T2a-Puro-MSCV vector (System Bioscience, Palo Alto, CA, USA). Lentivirus packaging and transduction were conducted as described previously.^{22,42} Cells stably expressing shCD9, shgp130, CD9-Flag or STAT3-C-Flag were enriched by puromycin selection for positive clones.

qRT-PCR. qRT-PCR was performed using a Bio-Rad CFX96 Real-Time PCR Detection System (Bio-rad, Hercules, CA, USA) or an ABI 7900HT Sequence Detection System (Applied Biosystems, Foster City, CA, USA) as previously described.^{8,44} The primer sequences were listed in Supplementary Table S6. Expression of *GAPDH* was used for the normalization.

Establishment of orthotopic GBM xenograft. Orthotopic GBM xenografts were established through intracranial implantation of GBM cells as previous described.^{8,42,48} Female C57BL/6 athymic/nude mice or NOG (NOD/Shi-scid/IL-2R γ null) immunocompromised mice of 4–6 weeks were purchased from Charles River Laboratories and were housed with no more than five animals per cage in a vivarium of Lerner Research Institute, Cleveland Clinic. Briefly, GSCs expressing luciferase were transduced with shCD9 and/or STAT3-C expressing vector or control vector, and then GSCs (D456 or T4121; 5×10^3 cells per mouse) were transplanted into the right frontal lobes of each mouse through intracranial injection (1 mm anterior, 2.5 mm lateral to the bregma and at a depth of 3.5 mm).

Bioluminescence imaging was applied to monitor the tumor growth using IVIS Spectrum system (PerkinElmer, Waltham, MA, USA) and data were quantified by Living Image Software (PerkinElmer, Waltham, MA, USA). Animals were maintained until manifestation of neurological signs. All *in vivo* experiments were carried out in accordance with the ARRIVE guidelines and the Guide for the Care and Use of Laboratory Animals and approved by the Institutional Animal Care and Use Committee of Cleveland Clinic.

Statistical analysis. Statistical analyses were performed using PASW Statistics 18 (SPSS Inc., Chicago, IL, USA) and GraphPad Prism 6 (GraphPad, La Jolla, CA, USA). Kolmogorov–Smirnov test was used to assess the normal distribution of data. Levene's test of homogeneity of variances was used to assess the variation within each group and the variance was similar among groups. Two-tailed unpaired *t*-test or one-way ANOVA were used to determine the level of significance, with $P < 0.05$ (*) and $P < 0.01$ (**) being considered with statistical significance. Bivariate correlation analysis (Pearson *r* test) was used to examine the correlation of two variables in human specimens. All data used in this study met the assumptions of statistical tests. No actions were taken to minimize the effects of subjective bias. The investigators were not blinded to allocation during experiments and outcome assessment. The *in vitro* and *in vivo* experiments included standard sample size based on prior studies.^{8,22,42,45} Neither samples nor animals were excluded from the analyses. Survival analyses were carried out using Kaplan–Meier method, with the log-rank test used for comparison. All quantitative data were presented as mean \pm S.D. or mean \pm S.E.M. as indicated.

Conflict of Interest

The authors declare no conflict of interest.

Acknowledgements. We thank the Department of Neurosurgery at Southwest Hospital and the Brain Tumor and Neuro-Oncology Center at Cleveland Clinic for providing GBM surgical specimens. We appreciate the technical support from Dr Sage O'Bryant of the Flow Cytometry Core, Drs Judith A Drazba and Eric Diskin of the Image Core, and Drs Belinda Willard and Ling Li of the Proteomics Laboratory at Lerner Research Institute, Cleveland Clinic. This research was supported by a China National Science and Technology Major Project (2016YFA0101203) to Xiu-Wu Bian and NIH R01 grants (CA184090 and NS091080) to Shideng Bao.

Author contributions

YS, X-WB and SB developed the hypothesis; YS, WZ, LC, X-WB and SB designed experiments and developed the methodology; YS, WZ, LC, CC, ZH, XF and ZH performed the experiments, collected and analyzed the data; QW, SX, JDL and YP provided reagents and technical assistance; YS wrote the manuscript; WZ, JNR, X-WB and SB revised the manuscript; SB and X-WB supervised the project.

1. Stupp R, Hegi ME, Mason WP, van den Bent MJ, Taphoorn MJ, Janzer RC *et al*. Effects of radiotherapy with concomitant and adjuvant temozolomide versus radiotherapy alone on survival in glioblastoma in a randomised phase III study: 5-year analysis of the EORTC-NCIC trial. *Lancet Oncol* 2009; **10**: 459–466.
2. Reardon DA, Wen PY. Glioma in 2014: unravelling tumour heterogeneity-implications for therapy. *Nat Rev Clin Oncol* 2015; **12**: 69–70.
3. Bao S, Wu Q, McLendon RE, Hao Y, Shi Q, Hjelmeland AB *et al*. Glioma stem cells promote radioresistance by preferential activation of the DNA damage response. *Nature* 2006; **444**: 756–760.
4. Chen R, Nishimura MC, Bumbaca SM, Kharbanda S, Forrest WF, Kasman IM *et al*. A hierarchy of self-renewing tumor-initiating cell types in glioblastoma. *Cancer Cell* 2010; **17**: 362–375.
5. Lathia JD, Mack SC, Mulkearns-Hubert EE, Valentim CL, Rich JN. Cancer stem cells in glioblastoma. *Genes Dev* 2015; **29**: 1203–1217.
6. Vermeulen L, Sprick MR, Kemper K, Stassi G, Medema JP. Cancer stem cells—old concepts, new insights. *Cell Death Differ* 2008; **15**: 947–958.
7. Li Z, Bao S, Wu Q, Wang H, Eyles C, Sathornsumetee S *et al*. Hypoxia-inducible factors regulate tumorigenic capacity of glioma stem cells. *Cancer Cell* 2009; **15**: 501–513.
8. Zhou W, Ke SQ, Huang Z, Flavahan W, Fang X, Paul J *et al*. Peritostin secreted by glioblastoma stem cells recruits M2 tumour-associated macrophages and promotes malignant growth. *Nat Cell Biol* 2015; **17**: 170–182.
9. Chen J, Li Y, Yu TS, McKay RM, Burns DK, Kernie SG *et al*. A restricted cell population propagates glioblastoma growth after chemotherapy. *Nature* 2012; **488**: 522–526.
10. Hemler ME. Targeting of tetraspanin proteins—potential benefits and strategies. *Nat Rev Drug Discov* 2008; **7**: 747–758.

11. Hemler ME. Tetraspanin proteins promote multiple cancer stages. *Nat Rev Cancer* 2014; **14**: 49–60.
12. Hemler ME. Tetraspanin functions and associated microdomains. *Nat Rev Mol Cell Biol* 2005; **6**: 801–811.
13. Sauer G, Windisch J, Kurzeder C, Heilmann V, Kreienberg R, Deissler H. Progression of cervical carcinomas is associated with down-regulation of CD9 but strong local re-expression at sites of transendothelial invasion. *Clin Cancer Res* 2003; **9**: 6426–6431.
14. Nakamoto T, Murayama Y, Oritani K, Boucheix C, Rubinstein E, Nishida M et al. A novel therapeutic strategy with anti-CD9 antibody in gastric cancers. *J Gastroenterol* 2009; **44**: 889–896.
15. Podergajs N, Motaln H, Rajcevic U, Verbosek U, Korsic M, Obad N et al. Transmembrane protein CD9 is glioblastoma biomarker, relevant for maintenance of glioblastoma stem cells. *Oncotarget* 2016; **7**: 593–609.
16. Higashiyama M, Taki T, Ieki Y, Adachi M, Huang CL, Koh T et al. Reduced motility related protein-1 (MRP-1/CD9) gene expression as a factor of poor prognosis in non-small cell lung cancer. *Cancer Res* 1995; **55**: 6040–6044.
17. Karlsson G, Rorby E, Pina C, Soneji S, Reckzeh K, Miharada K et al. The tetraspanin CD9 affords high-purity capture of all murine hematopoietic stem cells. *Cell Rep* 2013; **4**: 642–648.
18. Leung KT, Chan KY, Ng PC, Lau TK, Chiu WM, Tsang KS et al. The tetraspanin CD9 regulates migration, adhesion, and homing of human cord blood CD34+ hematopoietic stem and progenitor cells. *Blood* 2011; **117**: 1840–1850.
19. Kolle G, Ho M, Zhou Q, Chy HS, Krishnan K, Cloonan N et al. Identification of human embryonic stem cell surface markers by combined membrane-polysome translation state array analysis and immunotranscriptional profiling. *Stem Cells* 2009; **27**: 2446–2456.
20. Yu H, Pardoll D, Jove R. STATs in cancer inflammation and immunity: a leading role for STAT3. *Nat Rev Cancer* 2009; **9**: 798–809.
21. Hossain A, Gumin J, Gao F, Figueroa J, Shinjima N, Takezaki T et al. Mesenchymal stem cells isolated from human gliomas increase proliferation and maintain stemness of glioma stem cells through the IL-6/gp130/STAT3 pathway. *Stem Cells* 2015; **33**: 2400–2415.
22. Guryanova OA, Wu Q, Cheng L, Lathia JD, Huang Z, Yang J et al. Nonreceptor tyrosine kinase BMX maintains self-renewal and tumorigenic potential of glioblastoma stem cells by activating STAT3. *Cancer Cell* 2011; **19**: 498–511.
23. Kim E, Kim M, Woo DH, Shin Y, Shin J, Chang N et al. Phosphorylation of EZH2 activates STAT3 signaling via STAT3 methylation and promotes tumorigenicity of glioblastoma stem-like cells. *Cancer Cell* 2013; **23**: 839–852.
24. Wang H, Lathia JD, Wu Q, Wang J, Li Z, Hedderston JM et al. Targeting interleukin 6 signaling suppresses glioma stem cell survival and tumor growth. *Stem Cells* 2009; **27**: 2393–2404.
25. Gunther HS, Schmidt NO, Phillips HS, Kemming D, Kharbada S, Soriano R et al. Glioblastoma-derived stem cell-enriched cultures form distinct subgroups according to molecular and phenotypic criteria. *Oncogene* 2008; **27**: 2897–2909.
26. Ovalle S, Gutierrez-Lopez MD, Olmo N, Turnay J, Lizarbe MA, Majano P et al. The tetraspanin CD9 inhibits the proliferation and tumorigenicity of human colon carcinoma cells. *Int J Cancer* 2007; **121**: 2140–2152.
27. Hwang JR, Jo K, Lee Y, Sung BJ, Park YW, Lee JH. Upregulation of CD9 in ovarian cancer is related to the induction of TNF-alpha gene expression and constitutive NF-kappaB activation. *Carcinogenesis* 2012; **33**: 77–83.
28. Hu CC, Liang FX, Zhou G, Tu L, Tang CH, Zhou J et al. Assembly of urothelial plaques: tetraspanin function in membrane protein trafficking. *Mol Biol Cell* 2005; **16**: 3937–3950.
29. Tanaka Y, Tanaka N, Saeki Y, Tanaka K, Murakami M, Hirano T et al. c-Cbl-dependent monoubiquitination and lysosomal degradation of gp130. *Mol Cell Biol* 2008; **28**: 4805–4818.
30. Chondrogianni N, Petropoulos I, Grimm S, Georgila K, Catalgol B, Friguet B et al. Protein damage, repair and proteolysis. *Mol Aspects Med* 2014; **35**: 1–71.
31. Clague MJ, Urbe S. Ubiquitin: same molecule, different degradation pathways. *Cell* 2010; **143**: 682–685.
32. Morokoff A, Ng W, Gogos A, Kaye AH. Molecular subtypes, stem cells and heterogeneity: implications for personalised therapy in glioma. *J Clin Neurosci* 2015; **22**: 1219–1226.
33. Bollrath J, Pesses TJ, von Burstin VA, Putoczki T, Bennecke M, Bateman T et al. gp130-mediated Stat3 activation in enterocytes regulates cell survival and cell-cycle progression during colitis-associated tumorigenesis. *Cancer Cell* 2009; **15**: 91–102.
34. Howlett M, Judd LM, Jenkins B, La Gruta NL, Grail D, Ernst M et al. Differential regulation of gastric tumor growth by cytokines that signal exclusively through the coreceptor gp130. *Gastroenterology* 2005; **129**: 1005–1018.
35. Wang Y, Fuller GM. Phosphorylation and internalization of gp130 occur after IL-6 activation of Jak2 kinase in hepatocytes. *Mol Biol Cell* 1994; **5**: 819–828.
36. Graf D, Kohlmann C, Haselow K, Gehrman T, Bode JG, Haussinger D. Bile acids inhibit interleukin-6 signaling via gp130 receptor-dependent and -independent pathways in rat liver. *Hepatology* 2006; **44**: 1206–1217.
37. Hirano T, Matsuda T, Nakajima K. Signal transduction through gp130 that is shared among the receptors for the interleukin 6 related cytokine subfamily. *Stem Cells* 1994; **12**: 262–277.
38. Penuelas S, Anido J, Prieto-Sanchez RM, Folch G, Barba I, Cuatrecasas I et al. TGF-beta increases glioma-initiating cell self-renewal through the induction of LIF in human glioblastoma. *Cancer Cell* 2009; **15**: 315–327.
39. Inda MM, Bonavia R, Mukasa A, Narita Y, Sah DW, Vandenberg S et al. Tumor heterogeneity is an active process maintained by a mutant EGFR-induced cytokine circuit in glioblastoma. *Genes Dev* 2010; **24**: 1731–1745.
40. Chen H, Aksoy I, Gonnor F, Osteil P, Aubry M, Hamela C et al. Reinforcement of STAT3 activity reprogrammes human embryonic stem cells to naive-like pluripotency. *Nat Commun* 2015; **6**: 7095.
41. Chazaud B, Mouchiroud G. Inflamm-aging: STAT3 signaling pushes muscle stem cells off balance. *Cell Stem Cell* 2014; **15**: 401–402.
42. Cheng L, Huang Z, Zhou W, Wu Q, Donnola S, Liu JK et al. Glioblastoma stem cells generate vascular pericytes to support vessel function and tumor growth. *Cell* 2013; **153**: 139–152.
43. Friedman HS, Dolan ME, Moschel RC, Pegg AE, Felker GM, Rich J et al. Enhancement of nitrosourea activity in medulloblastoma and glioblastoma multiforme. *J Natl Cancer Inst* 1992; **84**: 1926–1931.
44. Shi Y, Chen C, Yu SZ, Liu Q, Rao J, Zhang HR et al. miR-663 suppresses oncogenic function of CXCR4 in glioblastoma. *Clin Cancer Res* 2015; **21**: 4004–4013.
45. Huang Z, Wu Q, Guryanova OA, Cheng L, Shou W, Rich JN et al. Deubiquitylase HAU5P stabilizes REST and promotes maintenance of neural progenitor cells. *Nat Cell Biol* 2011; **13**: 142–152.
46. Hu Y, Smyth GK. ELDA: extreme limiting dilution analysis for comparing depleted and enriched populations in stem cell and other assays. *J Immunol Methods* 2009; **347**: 70–78.
47. Fang X, Huang Z, Zhou W, Wu Q, Sloan AE, Ouyang G et al. The zinc finger transcription factor ZFX is required for maintaining the tumorigenic potential of glioblastoma stem cells. *Stem Cells* 2014; **32**: 2033–2047.
48. Bao S, Wu Q, Sathornsumetee S, Hao Y, Li Z, Hjelmeland AB et al. Stem cell-like glioma cells promote tumor angiogenesis through vascular endothelial growth factor. *Cancer Res* 2006; **66**: 7843–7848.

Supplementary Information accompanies this paper on Cell Death and Differentiation website (<http://www.nature.com/cdd>)